

The finite element method for the propagation of light in scattering media: Boundary and source conditions

M. Schweiger

Department of Medical Physics and Bioengineering, University College London, Capper Street, London, WC1E 6JA England

S. R. Arridge

Department of Computer Science, University College London, Gower Street, London, WC1E 6BT England

M. Hiraoka and D. T. Delpy

Department of Medical Physics and Bioengineering, University College London, Capper Street, London, WC1E 6JA England

(Received 20 December 1993; resubmitted 1 May 1995; accepted for publication 16 June 1995)

This paper extends our work on applying the Finite Element Method (FEM) to the propagation of light in tissue. We address herein the topics of boundary conditions and source specification for this method. We demonstrate that a variety of boundary conditions stipulated on the Radiative Transfer Equation can be implemented in a FEM approach, as well as the specification of a light source by a Neumann condition rather than an isotropic point source. We compare results for a number of different combinations of boundary and source conditions under FEM, as well as the corresponding cases in a Monte Carlo model.

Key words: diffusion equation, finite element method, 3D models, boundary conditions

I. INTRODUCTION

The development of a model to calculate light transport in highly scattering materials is essential for the assessment of measurements in diagnostic near-infrared spectroscopy (NIRS). Furthermore such a model is a key component in image reconstruction schemes to localize the optical properties of tissues from boundary measurements by solving the inverse problem.¹⁻⁴

The basic requirement of the model is to calculate the time-dependent light intensity, or its integral over time, at each point on the boundary of the object, when the source is an ultra-short light pulse (time-of-flight measurement),⁵ or to calculate the modulation depth and phase shift of the detected boundary signal, when the source is radio-frequency-intensity modulated.⁶ As only monochromatic laser sources are considered, and phosphorescence or inelastic scattering within the tissue can be neglected, a frequency-independent model of light transport is appropriate. This, of course, also holds for multi-wavelength systems, where the different frequencies are applied sequentially rather than simultaneously. The change in frequency is then simply expressed as a change in the optical properties of the tissue.

Previous results by a number of authors show that the diffusion approximation to the radiative transfer equation is a suitable model to describe light propagation in scatter-dominated materials.⁷⁻¹⁷ A model based on the Finite Element Method (FEM) to solve the diffusion equation numerically offers advantages in speed and flexibility in comparison with other models. In this paper we extend the techniques presented in Ref. 18 to accommodate more sophisticated boundary conditions that better match the physical problem. In so doing we demonstrate the power and flexibility of FEM for modelling photon transport in tissue.

In Sec. II, we give a brief revision of the Radiative Trans-

fer equation and its approximation by the Diffusion Equation. We show how a number of boundary conditions may be stated on the former leading to the corresponding conditions on the latter. These include Robin-type boundary conditions in addition to the previously applied Dirichlet-type boundary conditions, and the specification of the light source as a boundary current by a local Neumann boundary condition in addition to an isotropic point source. In Sec. III we revise the principles of the Finite Element Method, and show how our previous model is extended to accommodate five cases of boundary conditions and two different source specifications described in Sec. II. In Sec. IV we present results of all different source/boundary condition combinations for a particular geometry and homogeneous scattering and absorption properties, both for integrated intensity and for mean time-of-flight statistics. We also compare these results with an independent Monte Carlo model, with its own implementations of these different boundary conditions. In Sec. V we present discussion and conclusions.

II. THEORY

The aim of the photon transport model is to find the photon density Φ and the radiance I in a region Ω of strong scattering, and the outward current (exitance) Γ through its boundary $\partial\Omega$.

A common basis for the calculation of radiation propagation in absorbing and scattering media is the radiative transfer equation¹⁹ given by

$$\begin{aligned} \frac{1}{c} \frac{\partial I}{\partial t} + \hat{\mathbf{s}} \cdot \nabla I(\mathbf{r}, t, \hat{\mathbf{s}}) + (\mu_a + \mu_s) I(\mathbf{r}, t, \hat{\mathbf{s}}) \\ = \mu_s \int_{4\pi} f(\hat{\mathbf{s}}, \hat{\mathbf{s}}') I(\mathbf{r}, t, \hat{\mathbf{s}}') d^2 \hat{\mathbf{s}}' + q(\mathbf{r}, t, \hat{\mathbf{s}}), \end{aligned} \quad (1)$$

which describes the change of the radiance $I(\mathbf{r}, t, \hat{\mathbf{s}})$ at position \mathbf{r} into direction $\hat{\mathbf{s}}$. Here c is the velocity of light in the medium, μ_a and μ_s are the absorption and scattering coefficients, and $f(\hat{\mathbf{s}}, \hat{\mathbf{s}}')$ is the scattering phase function characterizing the intensity of a wave incident in direction $\hat{\mathbf{s}}'$ scattered into direction $\hat{\mathbf{s}}$. The scattering anisotropy is described by the average cosine \bar{f} of f . The values of \bar{f} for biological tissue are typically of the order of 0.9, indicating strongly forward biased scattering.

A well-known approximation to (1) widely used for light transport problems in highly scattering media is the diffusion equation, which can be expressed as²⁰

$$\frac{1}{c} \frac{\partial \Phi(\mathbf{r}, t)}{\partial t} - \nabla \cdot \kappa(\mathbf{r}) \nabla \Phi(\mathbf{r}, t) + \mu_a(\mathbf{r}) \Phi(\mathbf{r}, t) = q_0(\mathbf{r}, t), \quad (2)$$

where $\Phi(\mathbf{r})$ is the photon density at $\mathbf{r} \in \Omega$, $\kappa(\mathbf{r}) = [3(\mu_a(\mathbf{r}) + (1 - \bar{f})\mu_s(\mathbf{r}))]^{-1}$ is the diffusion coefficient, and $q_0(\mathbf{r})$ is an isotropic source distribution. The term $\mu'_s = (1 - \bar{f})\mu_s$ is referred to as the reduced scattering coefficient. It incorporates the effect of anisotropic scattering into the inherently isotropic diffusion approximation. A review of the method for deriving Eq. (2) from Eq. (1) is given in the Appendix.

The exitance Γ through $\partial\Omega$ at a point $\xi \in \partial\Omega$ is given by

$$\Gamma(\xi, t) = -c \kappa(\xi) \hat{\mathbf{n}} \cdot \nabla \Phi(\xi, t), \quad (3)$$

where $\hat{\mathbf{n}}$ is the normal to $\partial\Omega$ at ξ .

The diffusion approximation assumes $\mu_a \ll \mu_s$ and only weakly anisotropic light propagation. While the former condition is generally true for biological tissues, the latter is violated near sources and boundaries. However, comparisons of diffusion calculations with experiments²¹⁻²⁴ and Monte Carlo simulations²⁵⁻²⁷ performed by various authors show that qualitatively and, in certain cases, quantitatively correct predictions of boundary measurements can be obtained with diffusion models. Since our primary interest is in applying the light transport model to image reconstruction systems²⁸ where absolute quantitation is not essential, we can regard the diffusion equation as a valid model for calculating measurement signals.

The solution of Eq. (2) requires the specification of appropriate boundary conditions. Previously^{18,28} we have assumed the Dirichlet condition (DBC)

$$\Phi(\xi) = 0 \quad \forall \xi \in \partial\Omega. \quad (4)$$

Physically this is equivalent to a perfect absorbing medium surrounding the domain Ω . Each photon is immediately absorbed when crossing $\partial\Omega$ and thus the photon density equals zero outside Ω .

While this approach is commonly applied in literature,^{9,29} a more realistic approach leads to the boundary condition

$$\Phi(\xi) + 2\kappa \hat{\mathbf{n}} \cdot \nabla \Phi(\xi) = 0, \quad (5)$$

where $\hat{\mathbf{n}}$ is the normal to $\partial\Omega$ at ξ . This represents the physical model of a nonscattering medium surrounding Ω , assuming that no diffuse surface reflection at $\partial\Omega$ occurs. Equation (5)

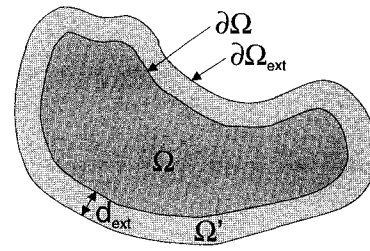


FIG. 1. Application of an extended boundary to an arbitrarily shaped domain Ω .

is a Robin boundary condition (RBC) which constrains a linear combination of the photon density and the current at $\partial\Omega$.

Equation (5) can be modified to incorporate a mismatch between the refractive indices n within Ω and n' in the surrounding medium. (In the following, we assume $n' = 1$.) Groenhuis *et al.*³⁰ derived the expression

$$\Phi(\xi) + 2\kappa \hat{\mathbf{n}} \cdot \nabla \Phi(\xi) = R[\Phi(\xi) - 2\kappa \hat{\mathbf{n}} \cdot \nabla \Phi(\xi)], \quad (6)$$

where R is a parameter governing the internal reflection at the boundary $\partial\Omega$. From a curve fit by Egan and Hilgeman,³¹ R can be approximated by

$$R \approx -1.4399n^{-2} + 0.7099n^{-1} + 0.6681 + 0.0636n. \quad (7)$$

From Eq. (6) a modified Robin boundary condition can be derived:

$$\Phi(\xi) + 2\kappa A \hat{\mathbf{n}} \cdot \nabla \Phi(\xi) = 0 \quad (8)$$

with $A = (1 + R)/(1 - R)$. Keijzer *et al.*¹⁶ use a different approach to derive A from Fresnel's laws as

$$A = \frac{2/(1 - R_0) - 1 + |\cos \theta_c|^3}{1 - |\cos \theta_c|^2}, \quad (9)$$

where $\theta_c = \arcsin(1/n)$ is the critical angle, and $R_0 = (n - 1)^2/(n + 1)^2$. For a value of $n = 1.4$ we get $A = 3.25$ and $A = 2.74$ for the Groenhuis and Keijzer algorithms, respectively. Setting $n = 1$ leads in both cases back to (5) without internal reflection.

While the RBC represents the physical situation more accurately than the DBC, the latter has the advantage of leading to a more simple mathematical model. A common compromise is to introduce an extrapolated boundary at a certain distance d_{ext} from the physical boundary at which the DBC is then applied. For an arbitrary 2D domain Ω the extrapolated boundary condition (EBC) is obtained by simply adding a border of thickness d_{ext} around Ω (see Fig. 1).

In the literature a number of expressions of extrapolation lengths for the one-dimensional problem are available, for both matched and mismatched refractive indices. These can be applied to arbitrary geometries if the radius of curvature of the boundary is small compared with the mean free path. For a matched boundary, Case and Zweifel³² give an approximation for the case $(1 - a) \ll 1$, where $a = \mu'_s/(\mu'_s + \mu_a)$:

$$d_{\text{ext}} \approx \frac{1}{\mu_s} 0.710446[1 - 0.0199(1 - a)^2]. \quad (10)$$

An expression for a mismatched boundary, based on Marshak's boundary condition, is given by Moulton:³³

$$d_{\text{ext}} = \sqrt{\frac{\kappa}{\mu_a}} \tanh^{-1}[2A \sqrt{\kappa \mu_a}]. \quad (11)$$

For typical values $\mu_a = 0.025 \text{ mm}^{-1}$ and $\mu_s' = 2.0 \text{ mm}^{-1}$, we get $d_{\text{ext}} = 0.355 \text{ mm}$ from Eq. (10), and $d_{\text{ext}} = 0.944 \text{ mm}$ from Eq. (11) for $n = 1.4$.

When modelling the light source incident at a point on the boundary, we distinguish two cases:

- (i) *Collimated source (CS)*: The diffusion equation cannot describe collimated sources correctly. A common approach is to represent a collimated pencil beam by an isotropic point source located at a depth $1/\mu_s'$ below the tissue surface. This produces accurate results at distances from the source larger than the mean free path, but breaks down close to the source.
- (ii) *Diffuse source (DS)*: For a diffuse source on the surface, the initial condition is naturally represented as an inward directed diffuse photon current distributed over the illuminated boundary segment $\partial\Omega_2 \subset \partial\Omega$.

The CS case leads to a δ -shaped source term q_0 in Eq. (2). Note that in the literature additional implementations of collimated sources are discussed. Eason et al.³⁴ give formulations for exponentially decaying line and cylinder sources. In nuclear engineering, a similar treatment known as *analytic uncollided flux method* is used for neutron transport calculations,³⁵ where the fluence is formed as the sum of an uncollided primary part and a collided part. While the exact modelling of the source is not very critical at large distances from the source compared to the mean free path length, simulations concerned with the light distribution close to the source will have to employ these more sophisticated source models.

The DS case can be incorporated directly into the boundary conditions. For DBC, the boundary condition (4) is then modified to be

$$\begin{aligned} \Phi(\xi, t) &= 0 & \forall \xi \in \partial\Omega_1, \\ \kappa(\xi) \hat{\mathbf{n}} \cdot \nabla \Phi(\xi, t) &= -\Gamma_s w(\xi, t) & \forall \xi \in \partial\Omega_2, \end{aligned} \quad (12)$$

where $\partial\Omega_1 \cup \partial\Omega_2 = \partial\Omega$, Γ_s is the strength of the source current, w is a weighting function, and $\hat{\mathbf{n}}$ is the outward normal to $\partial\Omega$ at ξ .

For the RBC, inclusion of the source as a photon current through the boundary is achieved by modifying the boundary condition (8) along $\partial\Omega_2$ to

$$\Phi(\xi, t) + 2\kappa A \hat{\mathbf{n}} \cdot \nabla \Phi(\xi, t) = -4\Gamma_s w(\xi, t) \quad \forall \xi \in \partial\Omega_2. \quad (13)$$

III. FINITE ELEMENT APPROACH

A finite element method is used to calculate solutions of the diffusion equation (2) together with boundary conditions (8) or (13). We seek a continuous and piecewise linear ap-

proximation Φ^h of Φ . To achieve this, we divide Ω into D nonoverlapping subdomains (*elements*) τ , over each of which Φ^h is assumed linear. *Nodes* N_j ($j = 1, \dots, P$) are attached to the element vertices. Φ^h at each point \mathbf{r} within an element τ_i is given by a linear interpolation of nodal values Φ_j ,

$$\Phi^h(\mathbf{r}, t) = \sum_{j|N_j \in \tau_i} \Phi_j(t) \psi_j(\mathbf{r}), \quad (14)$$

where ψ_j are linear nodal shape functions with support over all elements which have the node N_j as a vertex, and $\psi_j(\mathbf{r}_i) = \delta_{ij}$, where \mathbf{r}_i is the position of node N_i .

The weak formulation of (2) using the Galerkin approach is given by³⁶⁻³⁸

$$\begin{aligned} \int_{\Omega} \psi_j(\mathbf{r}) \left[\frac{1}{c} \frac{\partial}{\partial t} - \nabla \cdot \kappa(\mathbf{r}) \nabla + \mu_a(\mathbf{r}) \right] \Phi^h(\mathbf{r}, t) d\Omega \\ = \int_{\Omega} \psi_j(\mathbf{r}) q_0(\mathbf{r}) d\Omega \end{aligned} \quad (15)$$

for each node j . Integration by parts and substitution of Eq. (14) leads to

$$\begin{aligned} \int_{\Omega} \left[\psi_j(\mathbf{r}) \psi_i(\mathbf{r}) \frac{1}{c} \frac{\partial}{\partial t} \Phi_i(t) + \nabla \psi_j(\mathbf{r}) \cdot \kappa(\mathbf{r}) \nabla \psi_i(\mathbf{r}) \Phi_i(t) \right. \\ \left. + \mu_a(\mathbf{r}) \psi_j(\mathbf{r}) \psi_i(\mathbf{r}) \Phi_i(t) \right] d\Omega \\ = \int_{\Omega} \psi_j(\mathbf{r}) q_0(\mathbf{r}, t) d\Omega - \frac{1}{c} \int_{\partial\Omega} \psi_j(\xi) \Gamma(\xi, t) d(\partial\Omega). \end{aligned} \quad (16)$$

This can be written in matrix notation:

$$\mathbf{B} \frac{\partial \Phi}{\partial t} + [\mathbf{K}(\kappa) + \mathbf{C}(\mu_a)] \Phi = \mathbf{Q} - \beta. \quad (17)$$

The stationary problem $\partial\Omega/\partial t = 0$ can be solved directly, while for time-dependent problems the derivative is approximated by a finite difference scheme. If only the moments of the temporal distribution are requested, a fast algorithm presented elsewhere³⁹ can be used.

A. Implementation of boundary conditions

In the DBC-CS case (4), β vanishes in Eq. (17), as all shape functions ψ associated with boundary nodes are set to zero. The isotropic source distribution is defined by the value of \mathbf{Q} , which in the case of a point source [$q_0(\mathbf{r}) = \delta(\mathbf{r}, -\mathbf{r})$] has nonzero entries only for nodes associated with the element containing \mathbf{r}_s . In the case of RBC (8) and (13) the surface integral in Eq. (16) has to be calculated explicitly. If we define a general boundary condition as

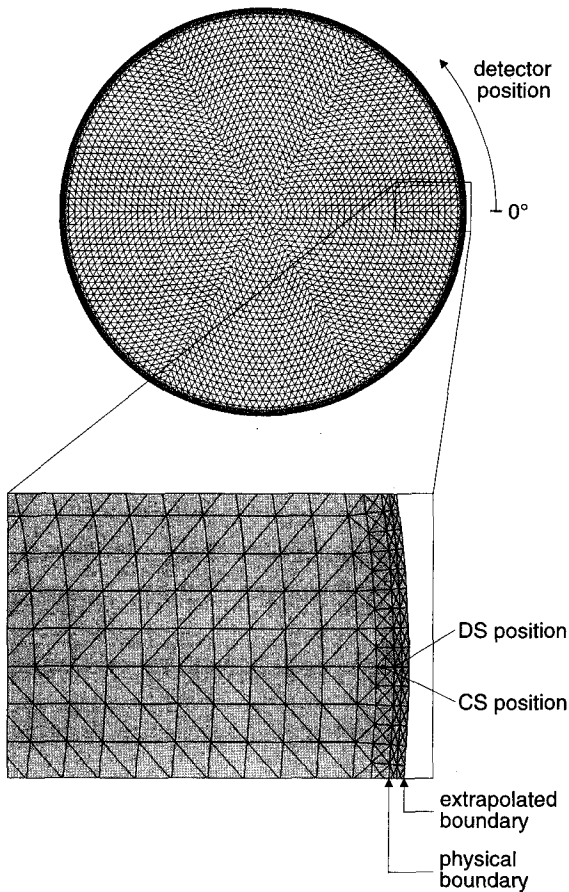


FIG. 2. Mesh structure for extended boundary FEM calculations.

$$\frac{\partial \Phi(\xi, t)}{\partial n} = f(\xi)\Phi(\xi, t) + g(\xi), \quad (18)$$

then together with Eq. (3) the surface integral in Eq. (16) can be written as

$$\begin{aligned} & \int_{\partial\Omega} \psi_j(\xi)\Gamma(\xi, t)d(\partial\Omega) \\ &= - \int_{\partial\Omega} \psi_j(\xi)c\kappa[f(\xi)\Phi(\xi, t) + g(\xi)]d(\partial\Omega). \end{aligned} \quad (19)$$

Using the boundary conditions for RBC-CS described above we obtain

$$\left. \begin{aligned} f(\xi) &= -\frac{1}{2\kappa(\xi)A} \\ g(\xi) &= 0 \end{aligned} \right\} \forall \xi \in \partial\Omega. \quad (20)$$

Equation (17) can then be modified to

$$\mathbf{B} \frac{\partial \Phi}{\partial t} + [\mathbf{K}(\kappa) + \mathbf{C}(\mu_a) + \mathbf{F}]\Phi = \mathbf{Q}, \quad (21)$$

where

$$F_{ij} = \frac{c}{2A} \int_{\partial\Omega} \psi_j(\mathbf{r})\psi_i(\mathbf{r})d(\partial\Omega) \quad (22)$$

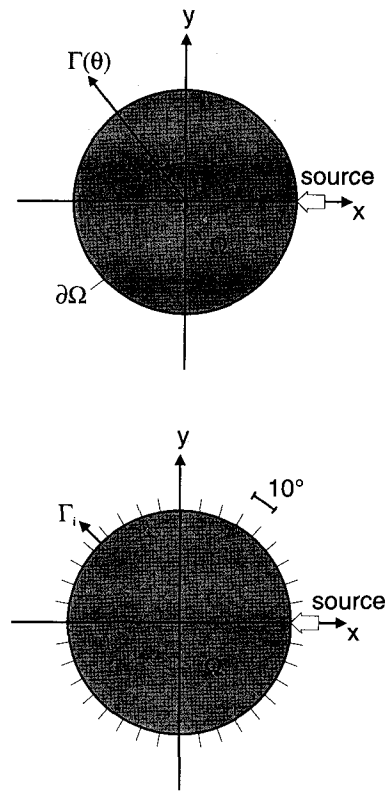


FIG. 3. Top: Model geometry for FEM simulations. Boundary measurements are given as a function of the angular output position. Bottom: Photon collection arrangement for MC exitance calculations.

and \mathbf{Q} is the isotropic source specification as in the DBC model.

For EBC, the FEM mesh is expanded by adding additional element layers around the boundary of the original mesh. The extended region has the same absorption and scattering properties as the physical region Ω . For the homogeneous cases discussed here this is trivial; for the inhomogeneous cases the optical properties of the additional elements would have to match those of the physical boundary segment they are attached to. The structure of the mesh and extended boundary is shown in Fig. 2. Once the extended mesh has been constructed, the solution Φ over Ω_{ext} can be obtained by the standard DBC FEM solver. The nonphysical solution

TABLE I. Identifiers for finite element model versions.

FEM model	Collimated source	Diffuse source
Dirichlet condition at boundary $\partial\Omega$	DBC-CS	DBC-DS
Dirichlet condition at extrapolated boundary $\partial\Omega_{\text{ext}}$, matched refractive index	EBC-CS	EBC-DS
Robin condition, matched refractive index	RBC-CS	RBC-DS
Dirichlet condition at extrapolated boundary, mismatched refractive index	EBCM-CS	EBCM-DS
Robin condition, mismatched refractive index	RBCM-CS	RBCM-CS

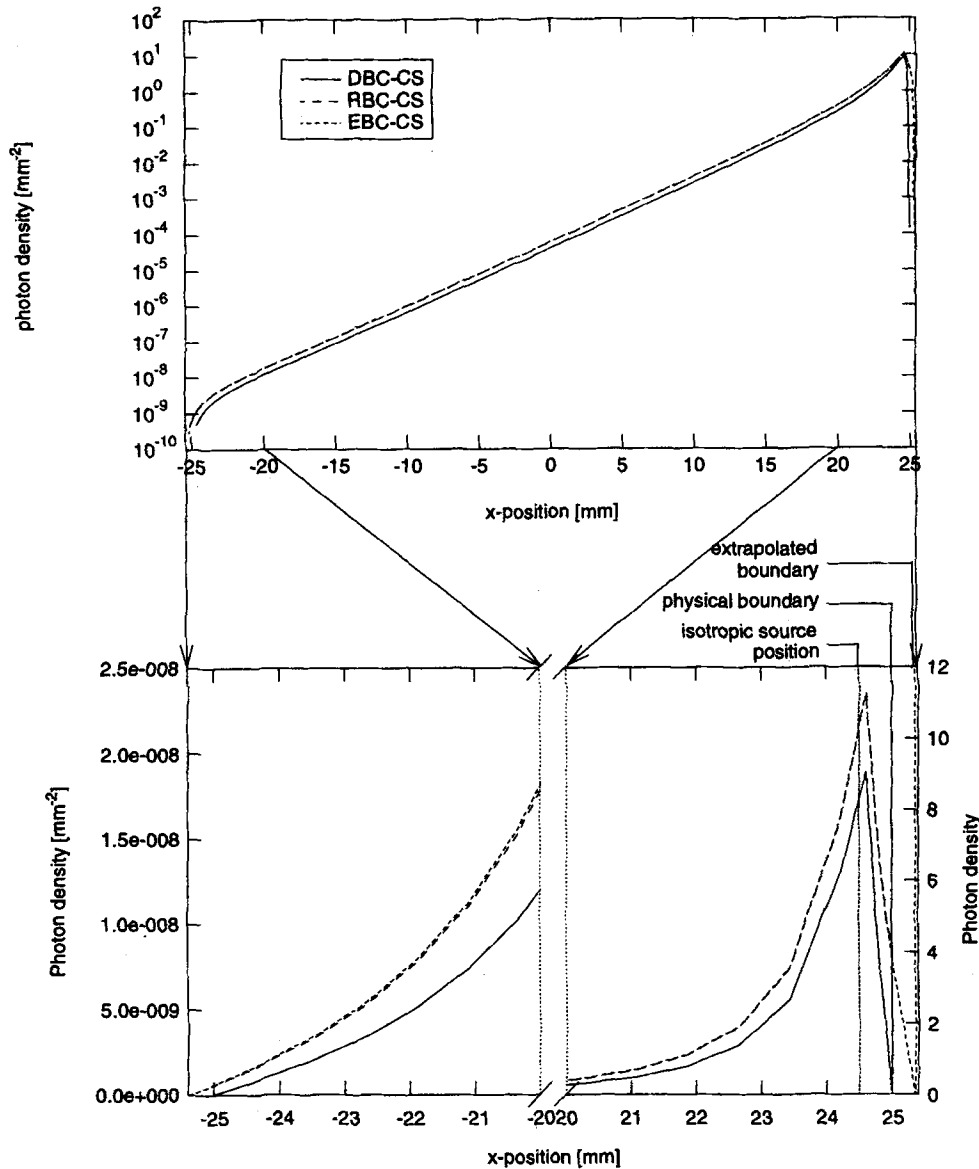


FIG. 4. Top: Photon density along the x -axis from $x = -25$ to $x = 25$ for DBC-CS, RBC-CS, and EBC-CS models on a logarithmic scale. Bottom: Magnifications of the sections close to the boundaries on a linear scale.

outside Ω is discarded. The exitance is given by Eq. (3), applied along the physical boundary $\partial\Omega$.

B. Implementation of source conditions

The treatment of the CS condition has been reported previously. An isotropic point source is placed at \mathbf{r}_s , located at $1/\mu'_s$ below the irradiance position, by initializing the three entries of \mathbf{Q} in Eq. (17) which are vertices of the element containing \mathbf{r}_s :

$$Q_i = q_s \psi_i(\mathbf{r}_s), \tag{23}$$

where q_s is the strength of the isotropic source.

If we consider a diffuse point source of strength $\Gamma_s(t)$ incident on $\xi_s \in \partial\Omega$, then in the DBC-DS case the surface

integral β is nonzero over the boundary segment containing ξ_s . In the discrete description, vector β has two nonzero entries:

$$\beta_i = -\Gamma_s(t) \psi_i(\xi_s), \tag{24}$$

where i enumerates the two boundary nodes bracketing ξ_s .

The application of the DS condition to the RBC model is achieved by setting the terms f and g in the general boundary condition (18) to

$$\left. \begin{aligned} f(\xi) &= -\frac{1}{2\kappa(\xi)A} \\ g(\xi) &= -\frac{2\Gamma_s}{\kappa(\xi)A} \delta(\xi - \xi_s) \end{aligned} \right\} \forall \xi \in \partial\Omega. \tag{25}$$

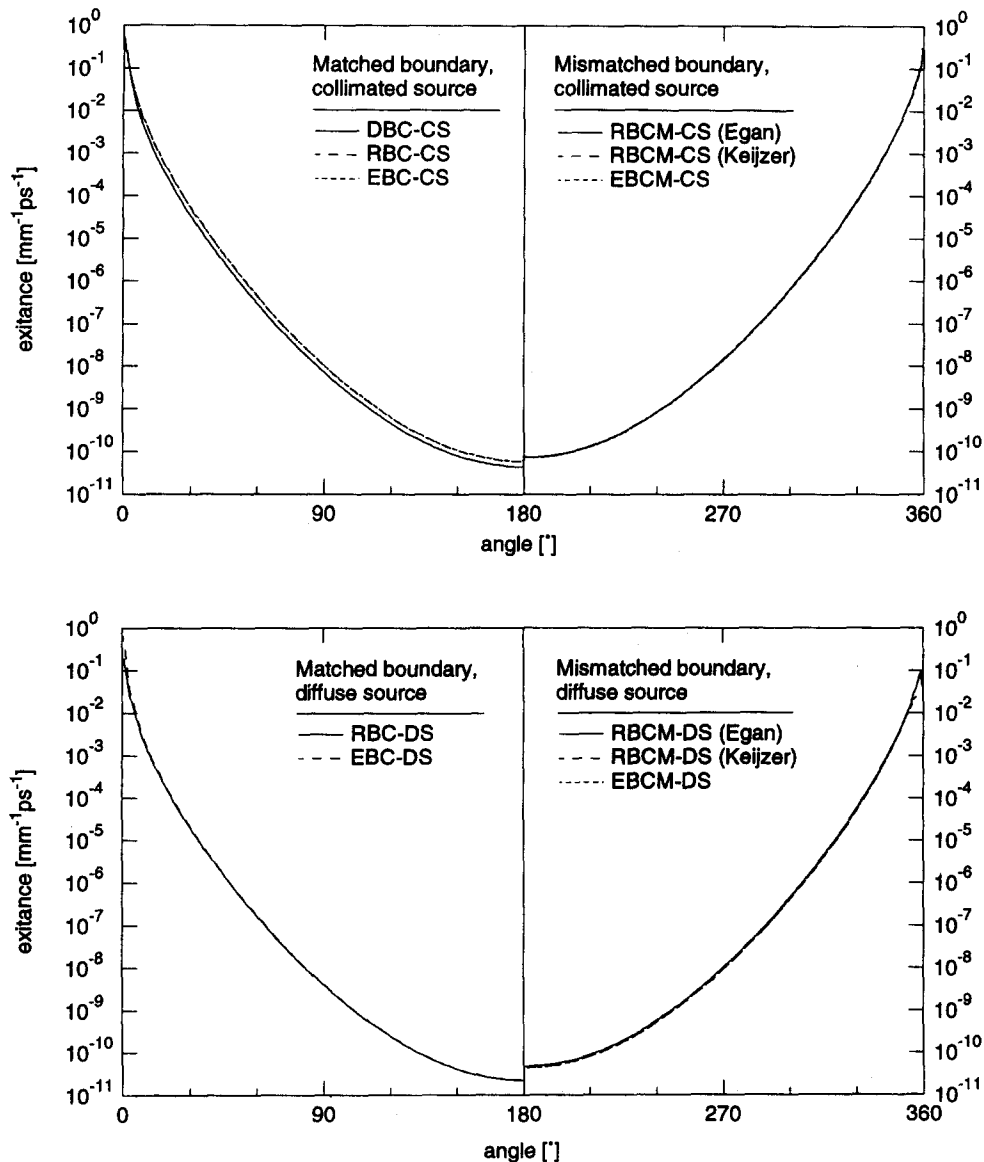


FIG. 5. The FEM exitance calculations. Top left: matched boundary/collimated source; top right: mismatched boundary/collimated source; bottom left: matched boundary/diffuse source; bottom right: mismatched boundary/diffuse source.

The source term Q in Eq. (21) for the RBC (13) is now given by

$$Q_i = \frac{2\Gamma_s}{A} \psi_i(\xi_s), \quad (26)$$

which is nonzero only for those boundary nodes enclosing the source position.

In the EBC models the diffuse source is obtained by placing an isotropic point source at the physical boundary.

In the case of a diffuse source we expect the solutions to be more accurate at small source-detector separations than for a collimated source, since a diffuse irradiance can be described exactly by the diffusion model, while the presence of a collimated source requires the unphysical representation by a diffuse source below the boundary, which is intended to give accurate results only at large distances. In terms of the FEM implementation the DS has the advantages that the

source placement does not depend on the value of μ'_s , and that the mesh no longer has to be locally refined around the source position to place it into an internal element.

IV. RESULTS AND DISCUSSION

We have implemented a FEM model which incorporates the boundary and source conditions discussed above and present results comparing the different cases. Specifically, we study

- (i) the errors produced by using a simple DBC model,
- (ii) the differences between RBC and EBC models,
- (iii) the effect of boundary mismatches, and
- (iv) the differences between CS and DS source conditions.

Finally a comparison with an independent Monte Carlo

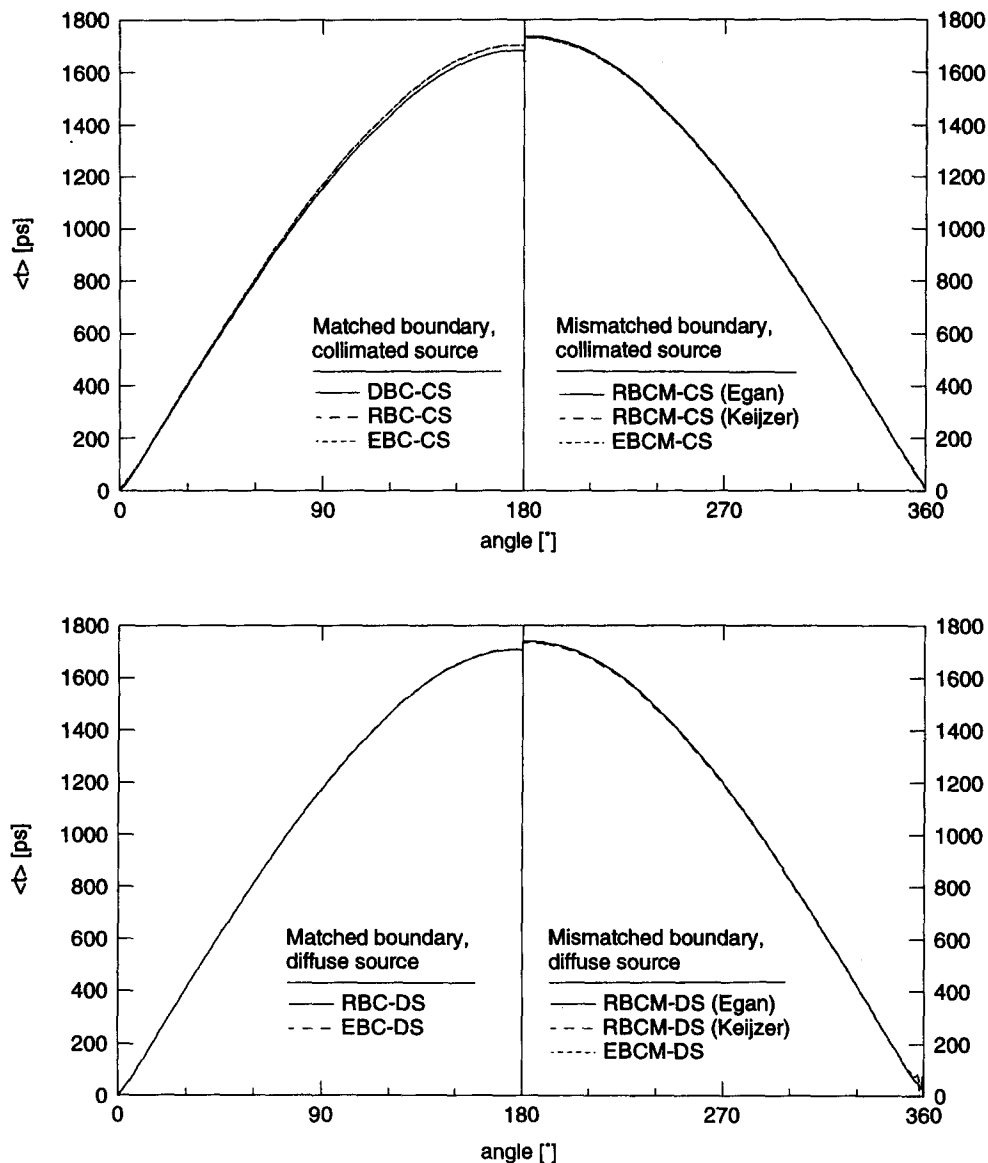


FIG. 6. The FEM mean time of flight calculations for the same cases as in Fig. 5.

(MC) model and with experimental data is performed to validate the FEM model.

For all FEM simulations a homogeneous circular 2D geometry is used. Although the FEM model is capable of handling complex inhomogeneous problems, for the purpose of this study a simple case is preferable to clarify the results. Figure 2 shows the mesh structure used for the simulations. For convenience, we place the mesh center at the coordinate origin, thus $\Omega = \{(x, y) | x^2 + y^2 \leq a^2\}$, where a is the mesh radius; a is set to 15 mm for the comparison of FEM and MC models (Sec. IV D), and to 25 mm for all other simulations. The measurement geometry for FEM simulations is shown in Fig. 3 (top). The optical parameters are set to $\mu_a = 0.025 \text{ mm}^{-1}$ and $\mu'_s = 2.0 \text{ mm}^{-1}$.

In the following, for the ease of discussion all FEM versions are referenced by identifiers listed in Table I. In all cases the source is an ultra-short light pulse incident at an-

gular position 0° on the surface. Since our main interest is the generation of the moments of the temporal distribution of the signal at the boundary, we present the results of the FEM models in terms of the integrated exitance and the mean time-of-flight as a function of the angular position of the detector. To further illustrate the differences between the various FEM flavors we also show the photon density distributions through the mesh along the x -axis (i.e., the diameter $y=0$). The internal solution itself is of interest in various problems such as the investigation of the effect of local parameter perturbations⁴⁰ or the calculation of Photon Measurement Density Functions.⁴¹ All exitance results are given as the number of photons per unit length (mm) per unit time (ps), normalized to an input strength of 1; all photon density results are given as the number of photons per unit area, again normalized to an input strength of 1.

A. Comparison of DBC, RBC, and EBC models

Figure 4 (top) shows the cross section through the photon density distribution along the x -axis for the DBC-CS, RBC-CS, and EBC-CS models, on a logarithmic scale. In all three cases the equivalent isotropic point source is placed at position (24.5, 0). Since due to the large dynamic range the differences between the models do not show up very well, the bottom graph shows enlargements of the results at sections close to the source and close to the opposite boundary, on a linear scale. We find that the RBC-CS and the EBC-CS results are virtually identical (about 0.5% difference), while the DBC-CS result is consistently lower with an approximately constant scaling factor of 0.7. Figures 5 and 6 show comparisons of exitance and mean time-of-flight data, respectively, calculated with the different FEM boundary models. We first study the top left graphs of both figures, containing the matched models DBC-CS, RBC-CS, and EBC-CS. For both exitance and mean time data we find again a very good agreement between RBC-CS and EBC-CS, while the DBC-CS differs significantly. Note that the absolute exitance variation between the models are higher than they appear due to the logarithmic scale. To highlight the differences, Fig. 7 shows the ratios RBC-CS/DBC-CS, EBC-CS/DBC-CS, and EBC-CS/RBC-CS for both exitance (top) and mean time (bottom). For exitance, the first two ratios both have a value of about 1.5 except close to the source, where DBC-CS produces higher values than the other models. For mean time, the differences between the FEM models are much less pronounced, with ratios of 1.01–1.02 for angles larger than 10° . Close to the source, DBC-CS drops significantly below the results of the other models.

These results lead to the conclusion that the Robin boundary model and the extrapolated boundary models are equivalent, and the choice may be based on the convenience of implementation for a given problem. The Dirichlet model, however, shows significant deviations, especially for exitance data. The only justification for DBC is the simplicity of its mathematical formulation, but the lack of accuracy will prevent its use in most applications.

B. The effect of boundary mismatches

We now investigate the influence of mismatches in the refractive indices of tissue and surrounding media. The models taking into account a boundary mismatch are RBCM-CS and EBCM-CS, where for RBCM-CS we test both choices of A from the Egan and the Keijzer approach [compare Eqs. (7) and (9)].

The results of the mismatched boundary models are compared with the matched boundary model RBC-CS (or, equivalently, EBC-CS). The top graph in Fig. 8 plots the photon densities calculated with the four models along the x -axis, and the bottom graph plots the ratios of each of the mismatched models with the matched model. We find that all mismatched models agree very well over the whole interval, in particular RBCM-CS and EBCM-CS. In the interior of the mesh all mismatched models are about a factor 1.5 higher

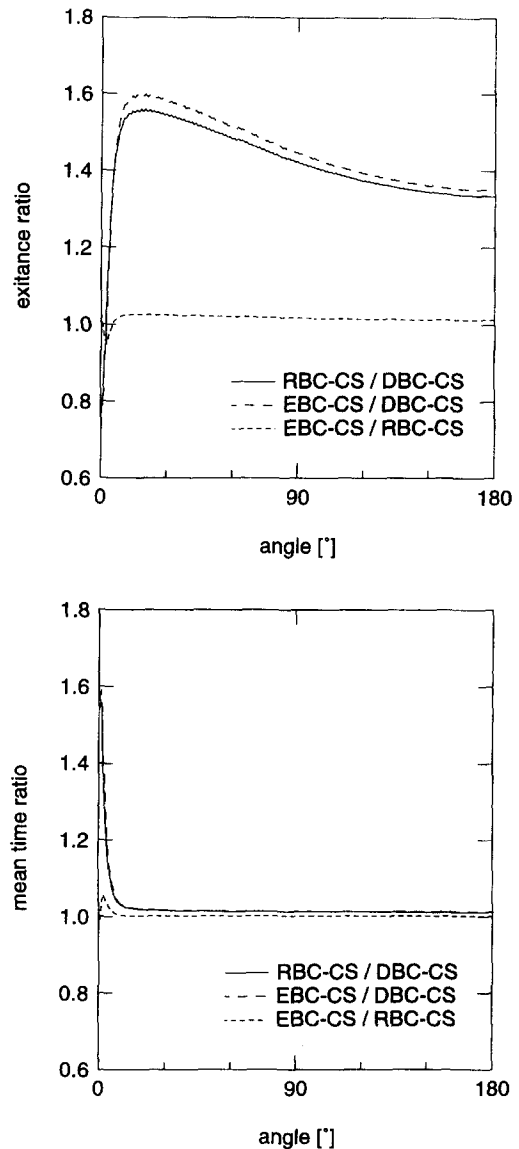


FIG. 7. Ratios of matched boundary/collimated source models with respect to DBC-CS. Top: Exitance. Bottom: Mean time.

than the matched model, with increasing deviations towards the boundaries.

The top right graphs in Figs. 5 and 6 show the exitance and mean time values of the mismatched models. All mismatched models are virtually indistinguishable among each other, but deviate from the matched models (compare with left graphs). Figure 9 plots the exitance and mean time ratios of the mismatched models with respect to RBC-CS. The differences between matched and mismatched models are more pronounced for exitance with ratios of 1.3–1.6 than for mean time with ratios of about 1.03 for angles larger than 15° .

We thus conclude that for the calculation of the solution in the interior, or for absolute exitance calculations, the effect of boundary mismatches is significant and cannot be neglected, even for large distances from the source.

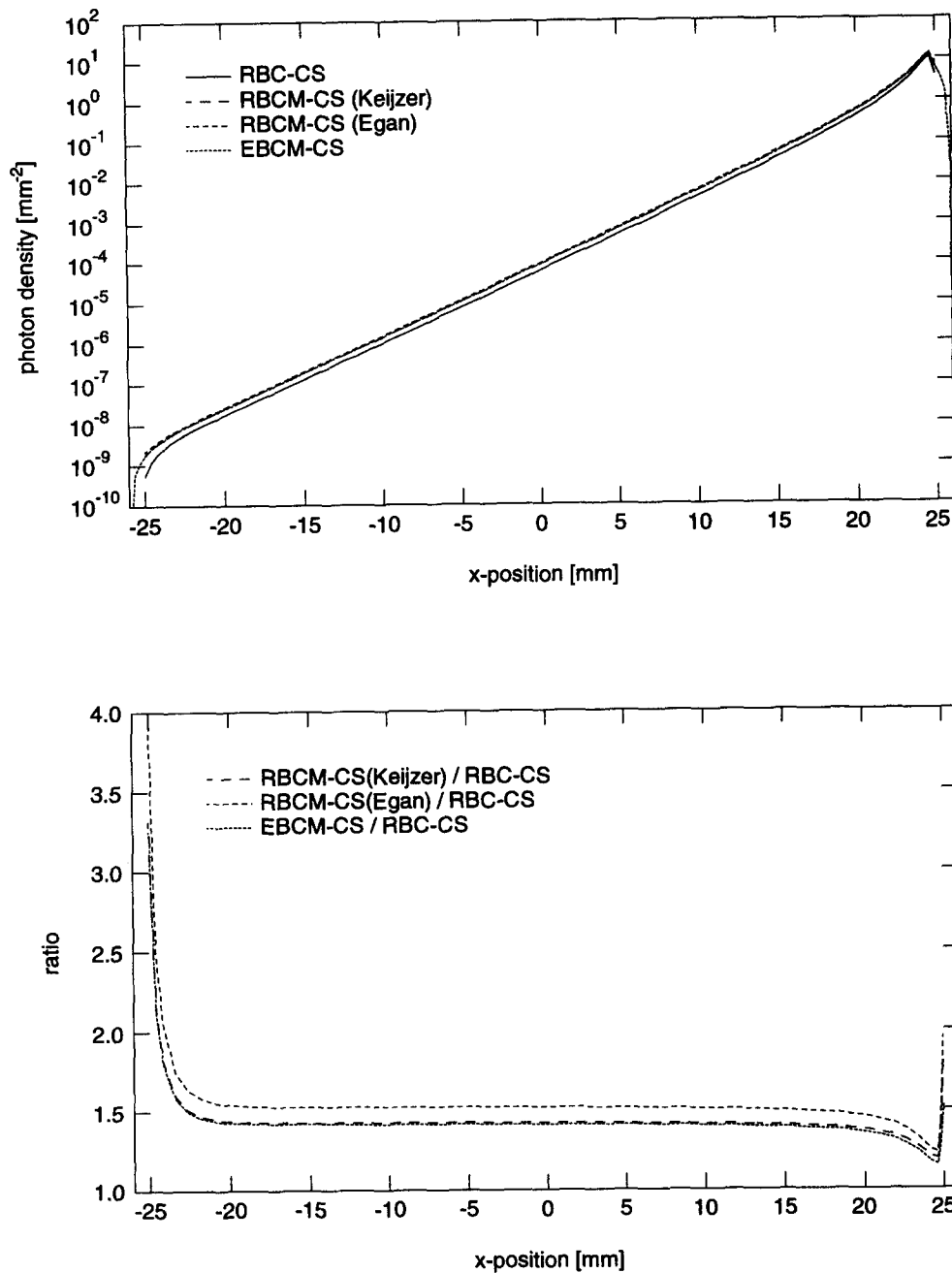


FIG. 8. Effect of boundary mismatches on the internal solution. Top: Photon density along the x -axis for RBC-CS, RBCM-CS (Keijzer and Egan methods), and EBCM-CS. Bottom: Ratios of mismatched models with respect to matched model RBC-CS.

C. The effect of source conditions

The influence of the source characteristic is investigated by comparing the collimated source (CS) models with their corresponding diffuse source (DS) counterparts. The bottom graphs of Figs. 5 and 6 show the exitance and mean time data from the different FEM models for DS conditions. The ratio of the DS models with respect to RBC-CS and with respect to the corresponding CS model is shown in Fig. 10.

For exitance, we find that the DS models produce lower values than the CS models with a ratio CS/DS of approximately 1.5 for the mismatched boundary models, and 2.5 for

the matched boundary models. When comparing the top left graph of Fig. 10 with the top graph of Fig. 9 one sees that the difference between matched and mismatched boundary models is larger for the DS case than for the CS case. This means that the application of appropriate boundary conditions is even more important for DS models.

For mean time, there is virtually no difference between DS and CS models for source-detector separations of more than 10° (Fig. 10, bottom right). This indicates that mean time measurements are less sensitive to source characteristics than exitance measurements. The differences between the

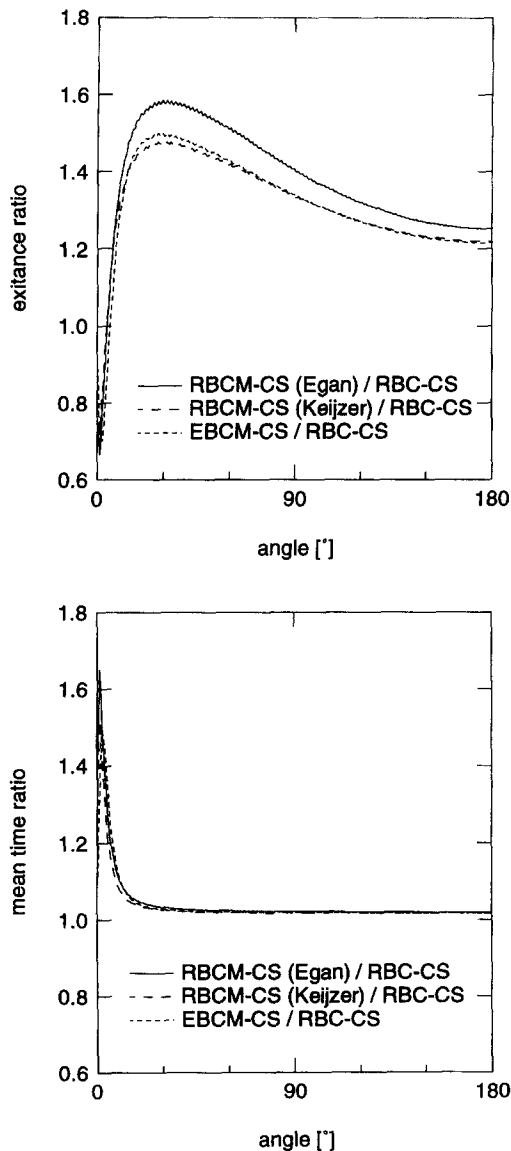


FIG. 9. Effect of boundary mismatches on boundary measurements: Ratios of mismatched boundary/collimated source models with respect to matched model RBC-CS. Top: Exitance Bottom: Mean time.

matched and mismatched boundary DS models (Fig. 10, bottom left) are comparable with those of the CS models (Fig. 9, bottom).

D. Comparison of FEM with Monte Carlo data

Previously⁴⁰ we have compared the Dirichlet version of the FEM model with an independent Monte Carlo (MC) model and found that the results for the mean time agree very well, while the exitance generated with the FEM model was up to 1.7 times as high as the MC model. One possible reason for this difference is the mismatch of boundary conditions, as the MC model takes into account surface reflection. To confirm this we perform a comparison of MC results including and excluding surface reflection with the corresponding versions of the FEM model.

The three-dimensional Monte Carlo model uses a cylindrical object $\Omega = \{(x,y,z) | (x^2 + y^2)^{1/2} < a\}$. A large collimated point source is incident in negative x -direction at the surface point $(a,0,0)$, and photons emitted from the surface are collected in 10° wide bins, according to their angular exit location, and integrated in the z -direction (see Fig. 3, bottom). This arrangement simulates a point source in combination with a line detector and is equivalent to the two-dimensional FEM model.⁴² For each 10° -bin i , the normalized exitance is given by sample

$$\Gamma_i = \frac{1}{N \cdot d} \sum_{j=1}^{N(i)} w_j, \tag{27}$$

where N is the total number of input photons and $N(i)$ is the number of output photons in bin i . Scaling factor $d=2.62$ mm is the arc length of the sampling area and w_j is the weight of photon j , which in this particular Monte Carlo implementation incorporates the effect of absorption.

Because of time restrictions the Monte Carlo models were for a smaller object than the previous results—a circle of radius 15 mm, with the same absorption and scattering coefficients as before. In all cases 10^7 photons were simulated.

Two types of boundary conditions are modelled, given by the rows in Table II. The first has no reflection effects included—all photons reaching the surface escape; this should approximate the RBC-CS and EBC-CS models. The second Monte Carlo condition employs a full Fresnel reflection model⁴³:

$$R = \frac{1}{2} \left[\frac{\sin^2(\theta_i - \theta_t)}{\sin^2(\theta_i + \theta_t)} + \frac{\tan^2(\theta_i - \theta_t)}{\tan^2(\theta_i + \theta_t)} \right], \tag{28}$$

where the angle of incidence θ_i and angle of transmittance θ_t are related by Snell's law

$$n \sin(\theta_i) = n' \sin(\theta_t), \tag{29}$$

where, as in Sec. II, n and n' are the refractive indices of the internal and external media, respectively. This model is the most sophisticated for Monte Carlo and can be compared to the RBCM-CS and EBCM-CS FEM models.

Figure 11 compares the results of both MC versions and their corresponding FEM models for both exitance and mean time. As expected, MC-noref corresponds very well with RBC-CS and EBC-CS, but not with DBC-CS for exitance. This confirms that indeed the discrepancies between MC and FEM DBC models reported previously are due to the oversimplified boundary condition in the FEM model, and that by using appropriate boundary conditions an excellent agreement between both models can be obtained.

When looking at the mismatched boundary results, we find a very good agreement of MC-ref with all of the mismatched FEM models RBCM-CS (Egan and Keijzer algorithms) and EBCM-CS.

The good agreement between the FEM and MC models substantiates the finding of other authors in the field that the diffusion approximation, although strictly not valid near boundaries, is still capable of producing quantitatively correct boundary measurement data for the type of problems encountered in optical transillumination.

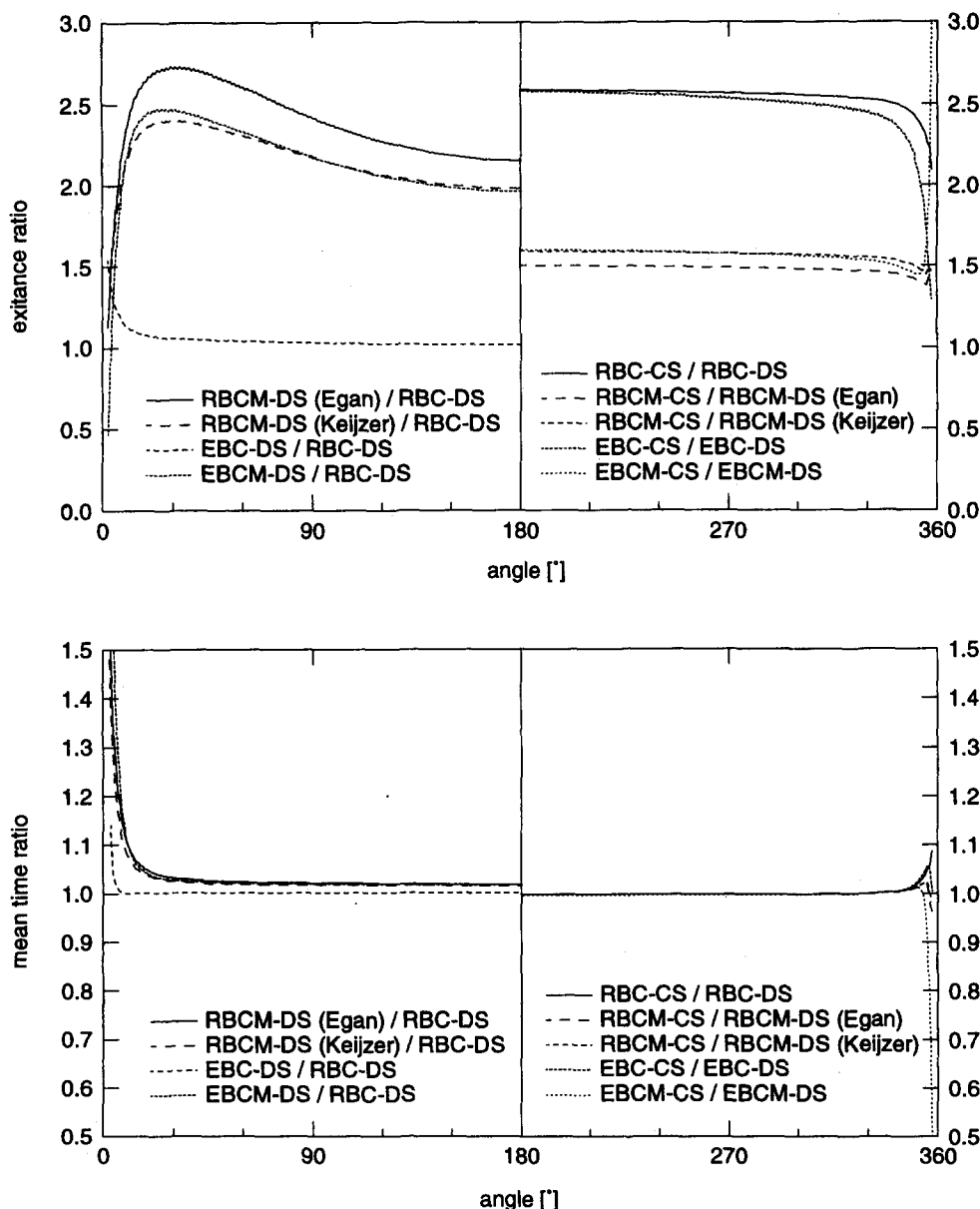


FIG. 10. Effect of source condition on boundary measurements. Top: exitance. Bottom: Mean time. The left graphs show the ratios of diffuse source models with respect to RBC-CS; the right graphs show the ratios of the diffuse and corresponding collimated source models.

V. CONCLUSIONS

Our aim in this paper has been to demonstrate the power of the finite element method in modelling both boundary conditions and source specification. Clearly the precise measurement values obtained depend quite significantly on the choices of these two specifications. The range of boundary conditions incorporated into the finite element procedure now allows us to select the model that matches a given ex-

perimental situation best. While the finite element method allows us to incorporate these improved boundary conditions with minimal additional computational effort, the speed of the Monte Carlo model is significantly reduced. This adds up to the huge advantage in processing speed of the finite element model reported previously.

More work will be required to find the conditions that correspond between real experiments and FEM. In particular, the source model requires more attention; neither the simple isotropic source at a depth of $1/\mu'_s$ nor the diffuse boundary current are appropriate. The correct model may have to take into account angular weighting, spatial distribution, and other factors. One way to approach this problem is the implementation of the analytic uncollided flux method mentioned above. Alternatively, a hybrid Monte Carlo diffusion model can be used, where the first scattering events are simulated

TABLE II. Identifiers for Monte Carlo model versions.

MC model	Collimated source
No internal reflection	MC-noref
Fresnel law	MC-ref

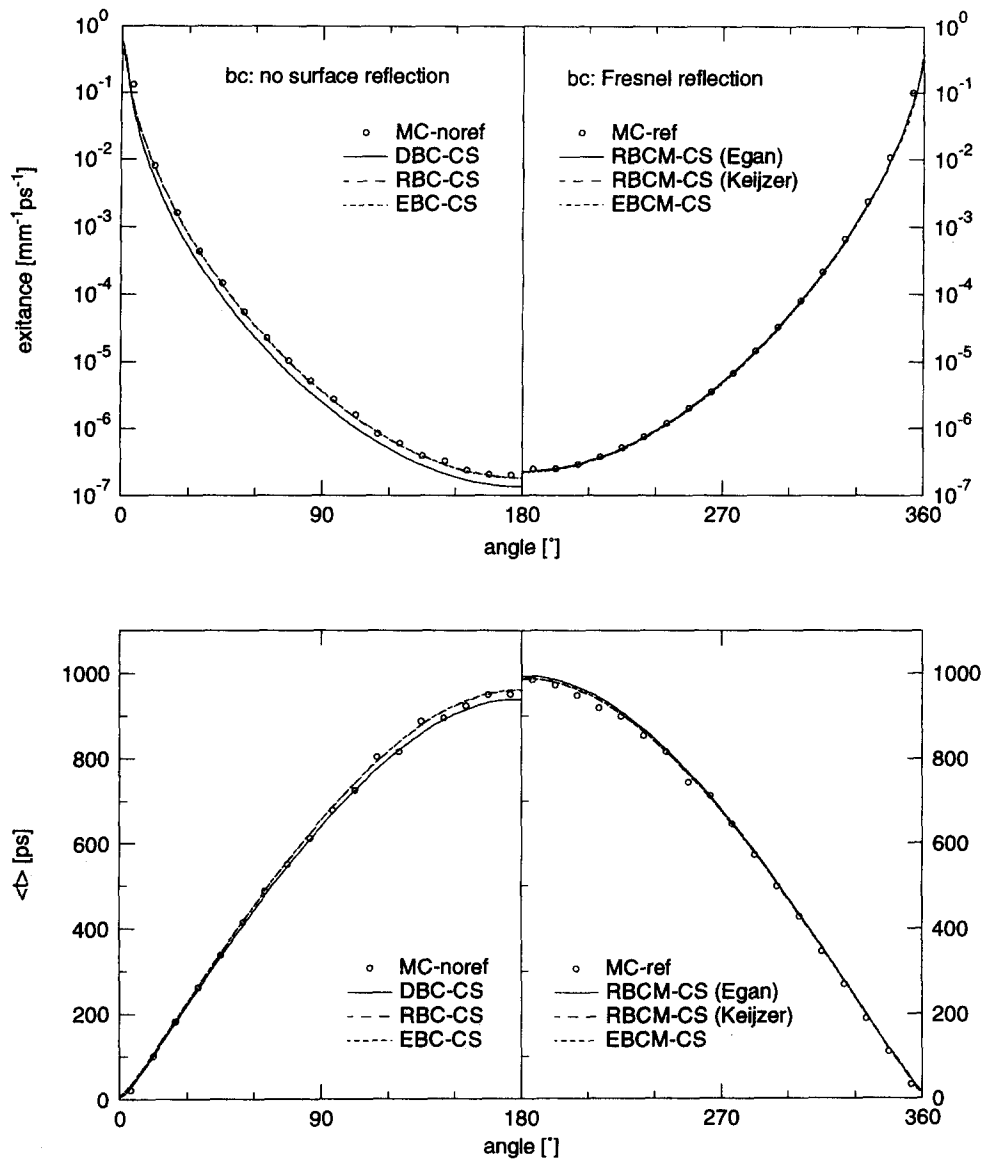


FIG. 11. Comparison of FEM and MC models with and without boundary reflections. Top: exitance. Bottom: Mean time. Left: Matched boundary. Right: Mismatched boundary.

by a MC model to generate a distributed, essentially isotropic source, which is then used as the starting point for the diffusion model.⁴⁴ To model realistic source conditions, the diffusion equation may have to be replaced by a higher-order approximation.

ACKNOWLEDGMENTS

This work was made possible by funding from the SERC, the Wellcome Trust, Action Research, and Hamamatsu Photonics KK.

VI. APPENDIX: REVIEW OF DIFFUSION APPROXIMATION

The Radiative Transfer Equation (RTE) (1) is a balance equation describing the change of energy radiance $I(\mathbf{r}, t, \hat{\mathbf{s}})$ in time due to changes in energy flow, loss due to absorption and scattering, and gain due to scattering and radiation

sources. I is defined so that the energy carried per unit time by photons in a unit solid angle $d^2\hat{\mathbf{s}}$ through an elemental area da given by its unit normal $\hat{\mathbf{n}}$, at position r , is given by

$$I(\mathbf{r}, t, \hat{\mathbf{s}}) \hat{\mathbf{s}} \cdot \hat{\mathbf{n}} da \quad d^2\hat{\mathbf{s}}. \tag{A1}$$

The exitance Γ through a unit area given by $\hat{\mathbf{n}}$ is obtained by integrating (A1) over all angles:

$$\Gamma(\mathbf{r}, t) = \int_{4\pi} I(\mathbf{r}, t, \hat{\mathbf{s}}) \hat{\mathbf{s}} \cdot \hat{\mathbf{n}} \quad d^2\hat{\mathbf{s}}. \tag{A2}$$

The diffusion approximation is commonly derived from the RTE by expansion of I into spherical harmonics and terminating after the first term, yielding³³

$$I(\mathbf{r}, t, \hat{\mathbf{s}}) = \frac{1}{4\pi} \Phi(\mathbf{r}, t) + \frac{3}{4\pi} \hat{\mathbf{s}} \cdot \mathbf{J}(\mathbf{r}, t), \tag{A3}$$

where Φ is the photon density

$$\Phi(\mathbf{r}, t) = \int_{4\pi} I(\mathbf{r}, t, \hat{\mathbf{s}}) d^2\hat{\mathbf{s}}, \quad (\text{A4})$$

and \mathbf{J} is the photon current

$$\mathbf{J}(\mathbf{r}, t) = \int_{4\pi} \hat{\mathbf{s}} I(\mathbf{r}, t, \hat{\mathbf{s}}) d^2\hat{\mathbf{s}}. \quad (\text{A5})$$

A similar expansion of the source term leads to

$$q(\mathbf{r}, t, \hat{\mathbf{s}}) = \frac{1}{4\pi} q_0(\mathbf{r}, t) + \frac{3}{4\pi} \hat{\mathbf{s}} \cdot \mathbf{q}_1(\mathbf{r}, t). \quad (\text{A6})$$

After substituting Eqs. (A3) and (A5) into the RTE and integrating over $\hat{\mathbf{s}}$ one can find the relations

$$\frac{1}{c} \frac{\partial \Phi}{\partial t} + \nabla \cdot \mathbf{J}(\mathbf{r}, t) + \mu_a \Phi(\mathbf{r}, t) = q_0(\mathbf{r}, t) \quad (\text{A7})$$

and

$$\left[\frac{1}{c} \frac{\partial}{\partial t} + \mu_a + \mu_s \right] \mathbf{J}(\mathbf{r}, t) = -\frac{1}{3} \nabla \Phi(\mathbf{r}, t) + \mathbf{q}_1(\mathbf{r}, t), \quad (\text{A8})$$

where μ'_s is the reduced scattering coefficient defined in the text.

To derive the diffusion equation, we make the assumptions

$$\mathbf{q}_1(\mathbf{r}, t) = 0, \quad (\text{A9})$$

$$\frac{1}{|\mathbf{J}|} \frac{\partial |\mathbf{J}|}{\partial t} \ll c(\mu_a + \mu'_s),$$

which simplifies Eq. (A8) to Fick's law

$$\mathbf{J}(\mathbf{r}, t) = -\kappa(\mathbf{r}) \nabla \Phi(\mathbf{r}, t). \quad (\text{A10})$$

By substituting this into Eq. (A7) one obtains the diffusion equation (2).

The correct boundary conditions for the problem described here demand that no photons come into the tissue through the surface (except at the source position):

$$I(\xi, t, \hat{\mathbf{s}}) = 0 \quad \forall \xi \in \partial\Omega, \quad \hat{\mathbf{s}} \cdot \hat{\mathbf{n}} < 0. \quad (\text{A11})$$

The diffusion equation cannot satisfy this condition exactly. Instead we assume that the total inward directed current is zero:

$$\int_{\hat{\mathbf{s}} \cdot \hat{\mathbf{n}} < 0} I(\xi, t, \hat{\mathbf{s}}) (\hat{\mathbf{s}} \cdot \hat{\mathbf{n}}) d^2\hat{\mathbf{s}} = 0 \quad \forall \xi \in \partial\Omega. \quad (\text{A12})$$

This leads to the boundary condition (5) in the text.¹⁹

To incorporate diffuse boundary reflection arising from a refractive index mismatch between the tissue and the surrounding medium, Eq. (A12) can be modified:

$$\int_{\hat{\mathbf{s}} \cdot \hat{\mathbf{n}} < 0} I(\xi, t, \hat{\mathbf{s}}) (\hat{\mathbf{s}} \cdot \hat{\mathbf{n}}) d^2\hat{\mathbf{s}} = \int_{\hat{\mathbf{s}} \cdot \hat{\mathbf{n}} > 0} R(\hat{\mathbf{s}}) I(\xi, t, \hat{\mathbf{s}}) (\hat{\mathbf{s}} \cdot \hat{\mathbf{n}}) d^2\hat{\mathbf{s}}, \quad (\text{A13})$$

where R is the refraction parameter defined in the text. From this the mismatched boundary condition (6) can be derived.

- ¹F. A. Grünbaum, P. D. Kohn, G. A. Latham, J. R. Singer, and J. P. Zubelli, "Diffuse tomography," *Proc. SPIE* **1431**, 232–238 (1991).
- ²S. R. Arridge, P. van der Zee, D. T. Delpy, and M. Cope, "Reconstruction methods for infra-red absorption imaging," *Proc. SPIE* **1431**, 204–215 (1991).
- ³S. R. Arridge, P. van der Zee, D. T. Delpy, and M. Cope, "Aspects of clinical infrared absorption imaging," in *The Formation, Handling, and Evaluation of Medical Images*, edited by A. T. Pokropek and M. A. Viergever, NATO ASI series F (Springer-Verlag, Heidelberg, 1992), pp. 407–418.
- ⁴S. R. Arridge, "The forward and inverse problems in time-resolved infrared imaging," in *Medical Optical Tomography: Functional Imaging and Monitoring*, edited by G. Muller, B. Chance, R. Alfano, S. Arridge, J. Beuthan, E. Gratton, M. Kashke, B. Masters, S. Svanberg, and P. van der Zee (SPIE, Bellingham, 1993), pp. 35–64.
- ⁵D. T. Delpy, M. Cope, P. van der Zee, S. R. Arridge, S. Wray, and J. Wyatt, "Estimation of optical pathlength through tissue from direct time of flight measurement," *Phys. Med. Biol.* **33**, 1433–1442 (1988).
- ⁶B. Chance, M. Maris, J. Sorge, and M. Z. Zhang, "A phase modulation system for dual wavelength difference spectroscopy of haemoglobin deoxygenation in tissue," *Proc. SPIE* **1204**, 481–491 (1990).
- ⁷A. Ishimaru, "Diffusion of light in turbid material," *Appl. Opt.* **28**(12), 2210–2215 (1989).
- ⁸J. C. Haselgrove, N. Guang, and B. Chance, "Investigation of the non-linear aspects of imaging through a highly scattering medium," *Med. Phys.* **19**, 17–23 (1992).
- ⁹M. S. Patterson, B. Chance, and B. C. Wilson, "Time resolved reflectance and transmittance for the noninvasive measurement of tissue optical properties," *Appl. Opt.* **28**(12), 2331–2336 (1989).
- ¹⁰B. W. Pogue and M. S. Patterson, "Frequency-domain optical absorption spectroscopy of finite tissue volumes using diffusion theory," *Phys. Med. Biol.* **39**, 1157–1180 (1994).
- ¹¹J. C. Schotland, J. C. Haselgrove, and J. S. Leigh, "Photon hitting density," *Appl. Opt.* **32**(4), 448–453 (1993).
- ¹²B. J. Tromberg, L. O. Svaasand, T.-T. Tsay, R. C. Haskell, and M. W. Berns, "Optical property measurements in turbid media using frequency domain photon migration," *Proc. SPIE* **1525**, 52–58 (1991).
- ¹³P. N. den Outer, T. M. Nieuwenhuizen, and A. Lagendijk, "Location of objects in multiple-scattering media," *J. Opt. Soc. Am. A* **10**(6), 1209–1218 (1993).
- ¹⁴J. P. Kaltenbach and M. Kaschke, "Frequency- and time-domain modeling of light transport in random media," in *Medical Optical Tomography: Functional imaging and Monitoring*, edited by G. Muller, B. Chance, R. Alfano, S. Arridge, J. Beuthan, E. Gratton, M. Kashke, B. Masters, S. Svanberg, and P. van der Zee (SPIE, Bellingham, 1993), pp. 65–86.
- ¹⁵J. L. Karagiannes, Z. Zhang, B. Grossweiner, and L. I. Grossweiner, "Applications of the 1-D diffusion approximation to the optics of tissues and tissue phantoms," *Appl. Opt.* **28**(12), 2311–2317 (1989).
- ¹⁶M. Keijzer, W. M. Star, and P. R. M. Storchi, "Optical diffusion in layered media," *Appl. Opt.* **27**(9), 1820–1824 (1988).
- ¹⁷J. C. Haselgrove, J. C. Schotland, and J. S. Leigh, "Long-time behavior of photon diffusion in an absorbing medium: application to time-resolved spectroscopy," *Appl. Opt.* **31**(15), 2678–2683 (1992).
- ¹⁸S. R. Arridge, M. Schweiger, M. Hiraoka, and D. T. Delpy, "A finite element approach for modeling photon transport in tissue," *Med. Phys.* **20**, 299–309 (1993).
- ¹⁹A. Ishimaru, *Wave propagation and scattering in random media* (Academic, New York, 1978), Vol. 1.
- ²⁰J. J. Duderstadt and L. J. Hamilton, *Nuclear Reactor Analysis* (Wiley, New York, 1976).
- ²¹S. Takatani and M. D. Graham, "Theoretical analysis of diffuse reflectance from a two-layer tissue model," *IEEE Trans. Biomed. Eng.* **BME-26**(12), 656–664 (1979).
- ²²S. J. Madsen, M. S. Patterson, B. C. Wilson, S. M. Jaywant, and A. Othonos, "Numerical modelling and experimental studies of light pulse propagation in inhomogeneous random media," *Proc. SPIE* **1888**, 90–102 (1993).
- ²³J. B. Fishkin and E. Gratton, "Propagation of photon-density waves in strongly scattering media containing an absorbing semi-infinite plane bounded by a straight edge," *J. Opt. Soc. Am. A* **10**(1), 127–140 (1993).
- ²⁴R. F. Bonner, R. Nossal, S. Havlin, and G. H. Weiss, "Model for photon migration in turbid biological media," *J. Opt. Soc. Am. A* **4**(3), 423–432 (1987).
- ²⁵L. Wang and S. L. Jacques, "Analysis of diffusion theory and similarity

- relations for light reflectance by turbid media," *Proc. SPIE* **1888**, 107–116 (1993).
- ²⁶L. Suddeath, V. Sahai, A. Wisler, C. Burch, B. Chance, and E. Sevick, "Finite element solution of the 'forward imaging' problem associated with time- and frequency-domain measurements of photon migration," *Proc. SPIE* **1888**, 117–128 (1993).
- ²⁷T. J. Farrell and M. S. Patterson, "A diffusion theory model of spatially resolved, steady-state diffuse reflectance for the noninvasive determination of tissue optical properties *in vivo*," *Med. Phys.* **19**, 879–888 (1992).
- ²⁸M. Schweiger, S. R. Arridge, and D. T. Delpy, "Application of the Finite-Element Method for the Forward and Inverse Models in Optical Tomography," *J. Math. Imag. Vision* **3**, 263–283 (1993).
- ²⁹S. J. Madsen, B. C. Wilson, M. S. Patterson, Y. D. Park, S. L. Jacques, and Y. Hefetz, "Experimental tests of a simple diffusion model for the estimation of scattering and absorption coefficients of turbid media from time-resolved diffuse reflectance measurements," *Appl. Opt.* **31**, 3909–3517 (1992).
- ³⁰R. A. J. Groenhuis, H. A. Ferwerda, and J. J. Ten Bosch, "Scattering and absorption of turbid materials determined from reflection measurements. 1: Theory," *Appl. Opt.* **22**(16), 2456–2462 (1983).
- ³¹W. G. Egan and T. W. Hilgeman, *Optical Properties of Inhomogeneous Materials* (Academic, New York, 1979).
- ³²K. M. Case and P. F. Zweifel, *Linear Transport Theory* (Addison–Wesley, Reading, MA, 1967).
- ³³J. D. Moulton, "Diffusion modelling of picosecond laser pulse propagation in turbid media," M. Eng. Thesis, McMaster University, Hamilton, Ontario (1990).
- ³⁴G. Eason, A. R. Veitch, R. M. Nisbet, and F. W. Turnbull, "The theory of back-scattering of light by blood," *J. Phys. D: Appl. Phys.* **11**, 1463–1479 (1978).
- ³⁵E. E. Lewis and W. F. Miller, Jr., *Computational Methods of Neutron Transport* (Wiley, New York, 1984).
- ³⁶O. C. Zienkiewicz and R. L. Taylor, *The finite element method*, 4th ed. (McGraw–Hill, London, 1987).
- ³⁷J. T. Oden and J. N. Reddy, *An introduction to the mathematical theory of finite elements* (Wiley, New York, 1976).
- ³⁸C. Greenough and K. Robinson, *Finite element library* (Numerical Algorithms Group, Rutherford Appellton Laboratory, Chilton, UK, 1981).
- ³⁹S. R. Arridge and M. Schweiger, "Direct calculation of the moments of the distribution of photon time of flight in tissue using a finite element method," *Appl. Opt.* **34** (15), 2683–2687 (1995).
- ⁴⁰M. Schweiger, S. R. Arridge, M. Hiraoka, and D. T. Delpy, "Application of the finite element method for the forward model in infrared absorption imaging," *Proc. SPIE* **1768**, 97–108 (1992).
- ⁴¹S. R. Arridge and M. Schweiger, "Photon Measurement Density Functions, Part II: Finite Element Calculations," *Appl. Opt.* (in press)
- ⁴²S. R. Arridge, M. Cope, and D. T. Delpy, "Theoretical basis for the determination of optical pathlengths in tissue: temporal and frequency analysis," *Phys. Med. Biol.* **37**, 1531–1560 (1992).
- ⁴³E. Hecht and A. Zajac, *Optics* (Addison–Wesley, Reading, MA, 1982).
- ⁴⁴L. Wang, and S. L. Jacques, "Hybrid model of Monte Carlo simulation Diffusion Theory for Light Reflectance by Turbid Media," *J. Opt. Soc. Am. A* **10**(8), 1746–1752 (1993).